algorithms

MDPI

Article

Fault Sensing Using Fractal Dimension and Wavelet

Mei Wang *, Liang Zhu and Yanan Guo

School of Electrical and Control Engineering, Xi'an University of Science and Technology, Xi'an 710054, China; m18712300931@163.com (L.Z.); gyn6523318@126.com (Y.G.)

* Correspondence: wangm@xust.edu.cn; Tel.: +86-29-85587613

Academic Editors: Javier Del Ser Lorente and Hsiung-Cheng Lin

Received: 25 August 2016; Accepted: 30 September 2016; Published: 11 October 2016

Abstract: A new fusion sensing (FS) method was proposed by using the improved fractal box dimension (IFBD) and a developed maximum wavelet coefficient (DMWC) for fault sensing of an online power cable. There are four strategies that were used. Firstly, the traditional fractal box dimension was improved to enlarge the feature distances between the different fault classes. Secondly, the IFBD recognition algorithm was proposed by using the improved fractal dimension feature extracted from the three-phase currents for the first stage of fault recognition. Thirdly, the DMWC recognition algorithm was developed based on the K-transform and wavelet analysis to establish the relationship between the maximum wavelet coefficient and the fault class. Fourthly, the FS method was formed by combining the IFBD algorithm and the DMWC algorithm in order to recognize the 10 types of short circuit faults of online power. The designed test system proved that the FS method increased the fault recognition accuracy obviously. In addition, the parameters of the initial angle, transient resistance, and fault distance had no influence on the FS method.

Keywords: fusion sensing; fault recognition; feature extraction; fractal dimension; wavelet; power cable

1. Introduction

It is important for power systems to run without faults. However, different types of faults often occur [1,2].

In neutral grounded power systems, single-phase ground faults account for 70%–80%, two-phase faults and two-phase ground faults account for 10%, and three-phase faults account for 5% of all faults that occur. Ground faults account for 90% of cases and the single-phase ground faults account for 84% of cases [3–5].

In most of the literature, the online cable recognition methods concentrate on fractal theory, wavelet transform, neural network, genetic algorithms, and chaos theory. However, the research results can only be achieved in laboratory conditions [6].

Fractal methods have developed rapidly in recent years due to good adaptation and good cross properties [7–9]. Scientists often combine it with other methods for signal processing [10]. More and more scholars are studying the fault diagnosis methods for power systems by combining fractal theory with other theories. For example, one research group used fractal theory and spectral analysis to select the single-phase fault phase in a small current grounded system [11]. In addition, researchers have compared the fractal dimensions of the transient currents between the fault phase and the non-fault phase to recognize the single-phase fault [12,13]. Other researchers studied the state features of the transient signals of the high frequencies; these signals were caused by power system faults. The researchers combined the chaos theory with the fractal theory to analyze and classify the operational state of the power system [14–17].

On the other hand, wavelet theory is one of the outstanding achievements of mathematics research. It has been applied extensively in non-linear field theory. Wavelet analysis possesses localized

characteristics in the time-frequency domain. It can highlight mutative components of the processed signals by flexibly changing the window of the time-frequency domain, and can then extract the power cable fault information effectively [18–21]. After comparing the wavelet modulus difference of the target traveling wave from the two ends, the fault type can be recognized [22]. However, this method fails to select the faulty phases of two-phase grounded faults. However, the fault type could be recognized according to the relationship between the amplitudes of the current modules [23]. Another study proposed a fault location method based on the genetic algorithm using the transient components of three-phase currents [24]. These methods have made great contributions to fault detection in power systems. However, these methods are still in the theoretical stages and have not been used in practice.

Based on the aforementioned methods, a new fusion sensing (FS) method was proposed by using the improved fractal dimension and a developed maximum wavelet modulus for short-circuit fault recognition of online power cables in this paper.

The organization of this paper is as follows: Short-circuit fault components in online power cables are described in Section 2. The improved fractal box dimension (IFBD) recognition algorithm is proposed in Section 3. The developed maximum wavelet coefficient (DMWC) recognition algorithm is described in Section 4. The FS method is proposed by combining the IFBD algorithm and the DMWC algorithm in Section 5. The analysis of the experiment and the results are reported in Section 6, which includes three cases of different initial angles, different transient resistances, and different fault distances. The conclusions are drawn in Section 7.

2. Description of Short-Circuit Fault Components in Online Power Cable

The main classes of short-circuit faults in the three-phase power cable system and their voltage and current characteristics are shown in Table 1.

Table 1. Classes of short-circuit faults and their characteristics.

Class	Schematic Diagram of Fault	Characteristics
Three-phase grounded fault of A, B and C	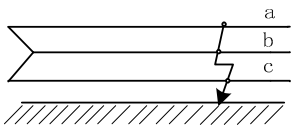	$U_A = U_B = U_C = 0$
Phase-between fault of B and C	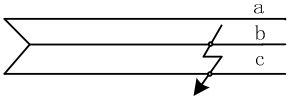	$U_A\uparrow$, $I_B = I_C = 0$
Single-phase grounded fault of A	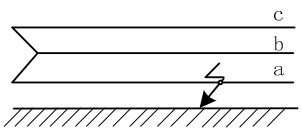	$I_A\uparrow$, $I_B = I_C = 0$
Two-phase grounded fault of B and C	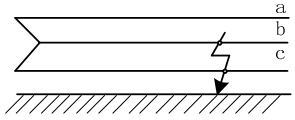	$I_A = 0$, $I_B\uparrow$, $I_C\uparrow$

If a short-circuit fault of the three phases occurred, the voltage of each phase would be reduced. If a single-phase fault occurred, the fault phase current would increase, and the currents of the non-fault phases would decrease. The same class of faults has the same features, and different classes of faults have different features [25,26]. The power cable fault state (PCFS) can be denoted by the sum of the normal state (NS) and the fault component state (FCS), as indicated in Equation (1) and Figure 1.

$$\text{FCS} = \text{PCFS} - \text{NS} \tag{1}$$

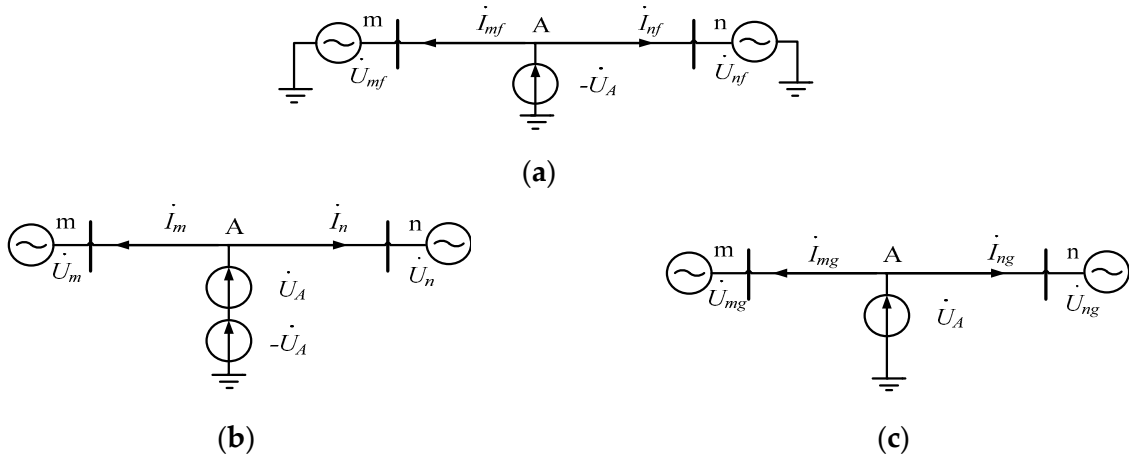

Figure 1. Power cable states of (**a**) fault component state (FCS); (**b**) power cable fault state (PCFS); and (**c**) normal state (NS).

The fault components exist in the added abnormal state of the power cable. The voltage of the fault components can be obtained by the differences between the cable voltage after fault occurrence and the voltage of the normal state. Similarly, the current of the fault components can be obtained by the differences between the cable current after fault occurrence and the current of the normal state.

In a practical system of an online power cable, the n periods of voltage or current before fault occurrence are regarded as the voltage or current of the normal state. The voltage or current of the fault components $S_g(t)$ can be calculated as follows [27].

$$S_g(t) = S(t) - (-1)^n S(t - nT/2) \tag{2}$$

where $S(t)$ is the voltage or the current after fault occurrence, T is the power frequency period, and n is a positive natural number (usually, $n = 2$).

The fault component is the voltage difference or current difference of a period. The fault component should also satisfy the time requirement for fault recognition.

The fault component of the current was taken as the initial signals of the power cable fault in this paper. We used Equation (1) to obtain the fault components of the power cable in the 10 types of short-circuit states. It includes three types of single-phase faults, three types of two-phase faults, three types of two-phase grounded faults, and one type of three-phase faults. The three phase currents and their fault components of the single-phase A earth faults are shown in Figure 2. The blue curves are for phase A, the red curves are for phase B, and the green curves are for phase C.

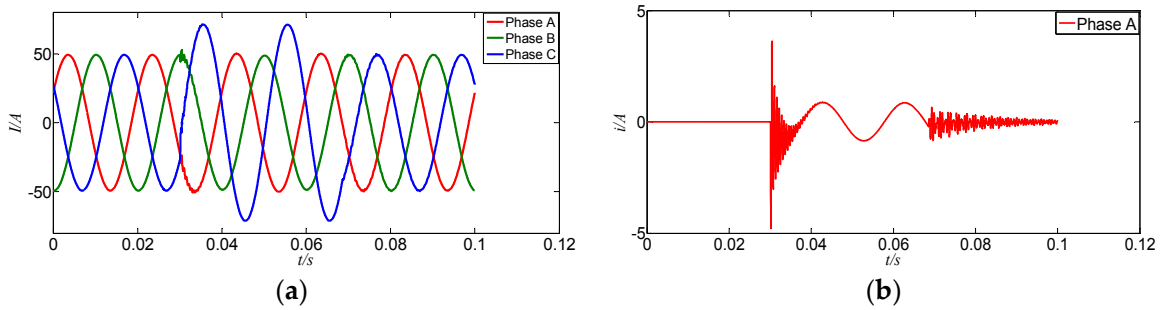

Figure 2. *Cont.*

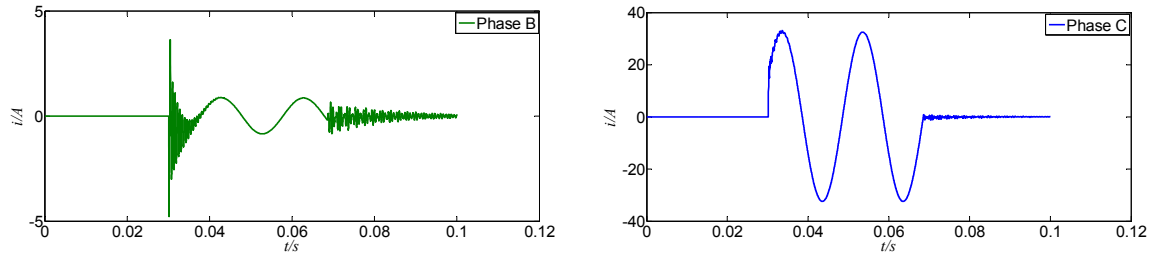

Figure 2. (**a**) Three-phase currents of a single-phase *A* grounded fault; (**b**) Fault component of phase *A*; (**c**) Fault component of phase *B*; (**d**) Fault component of phase *C*.

3. The Improved Fractal Box Dimension (IFBD) Recognition Algorithm

The fractal dimension can effectively measure the change of the fine distributed signals, and it keeps invariant if the signals are processed at different scales. Particularly, the box dimension is more suitable for use in calculating a figure or a discrete sport set. Therefore, the box dimension was chosen in this paper as the base to extract the fault feature [28–30].

3.1. Definition of the Improved Fractal Box Dimension

The traditional box dimension $Dim\ (S_r)$ of the point set S_r in a linear space R^n is

$$Dim\ (S_r) = \lim_{n\to\infty} \frac{lnN_n\ (S_r)}{ln2^n} \tag{3}$$

where n is the length of a side of a square box which covers the point set S_r. $N_n(S)$ represents the minimum number of boxes containing S_r.

By using the above approximation method, the box dimensions of the fault components of phase *A*, phase *B*, and phase *C* are calculated in the condition of the phase *A* earth fault shown in Figure 1. $Dim\ (S_A)$ = 1.56030, $Dim\ (S_B)$ = 1.57527, $Dim\ (S_C)$ = 1.54622.

For the curves in a plane, their box dimensions always range from one to two. To make the fault classification easier, we can enlarge the distances between the different classes of the 10 types of the short circuit faults. Based on experiments, we defined the improved box dimension F as follows.

$$F = \tan\frac{Dim(S)}{E(Dim^*)} \tag{4}$$

where "tan" represents the tangent function, and $E(Dim^*)$ is the expectation of the traditional box dimension Dim of the phase current in the normal state, and it can be written as follows.

$$E(Dim^*) = \frac{1}{m}\sum_{r=1}^{m} Dim\ (S_r) \tag{5}$$

where S_r is the current signals of the power cable in normal state, $r = 1, 2, \cdots, m$, and m is a positive integer greater than three.

According to Equation (4), we have the improved box dimensions F_A, F_B, and F_C of the fault components of the three phase currents.

$$F_A = \tan\frac{Dim(S_A)}{E(Dim^*)} \tag{6}$$

$$F_B = \tan\frac{Dim(S_B)}{E(Dim^*)} \tag{7}$$

$$F_C = \tan\frac{Dim(S_C)}{E(Dim^*)} \tag{8}$$

where $Dim(S_A)$, $Dim(S_B)$, and $Dim(S_C)$ are the traditional box dimensions of the currents of phase A, B, and C, respectively. $E(Dim^*)$ is the expectation of the traditional box dimension Dim of the phase current in the normal state. "tan" represents the tangent function.

For the 10 detailed classes of the short circuit faults, the fault features using the traditional box dimension and the improved box dimension are shown in Figure 3a,b respectively. The horizontal axis represents the short circuit faults which include the 10 classes of short circuit faults. *AG*, *BG*, and *CG* are the single-phase short circuit faults. *AB*, *BC*, and *AC* are the phase-between short circuit faults. *ABG*, *BCG*, and *ACG* are the double-phase short circuit faults. *ABC* is the three-phase short circuit fault. The vertical axis is the fault feature values. The blue color represents phase *A*, the green color represents phase *B*, and the red color represents phase *C*.

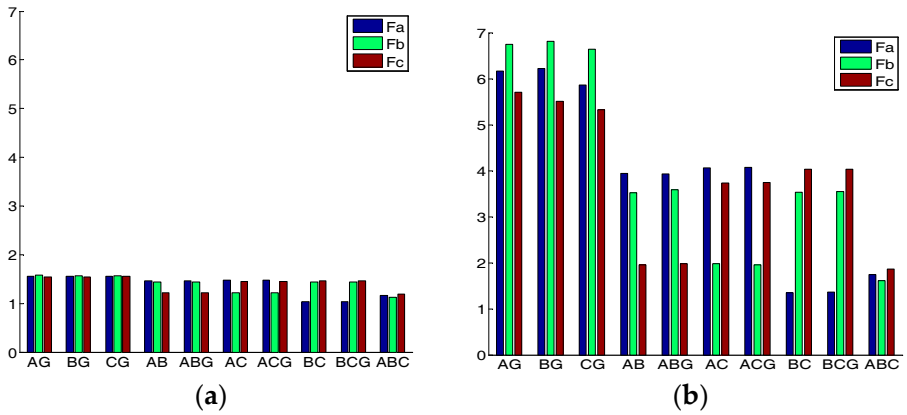

Figure 3. Fault feature histogram of the 10 types of short circuit faults by using (**a**) the traditional box dimension; and (**b**) the improved box dimension.

From Figure 3, it is clear that the traditional box dimension features of the 10 classes are relatively crowded. Compared to the traditional box dimension features, the improved box dimension features of the 10 classes have larger distances among the single-phase fault and the double-phase fault, as well as the three-phase fault. Furthermore, the improved box dimension features have larger distances among the different single-phase faults of *A*, *B*, and *C*. Obviously, the improved box dimension feature is better for short circuit fault recognition of the online power cable than the traditional box dimension feature.

3.2. The Improved Fractal Box Dimension (IFBD) Recognition Algorithm

According to the improved box dimension of Equations (6)–(8), we calculated the improved box dimension features of the short circuits. Based on the calculation results, we found the relationship between the fault classes and the IFBD features, shown in Table 2 below. We found that the improved box dimension features have a similar relationship in the cases of the two-phase grounded faults and the two-phase-between faults. After the three phase currents or voltages were collected, we could use the relationship to classify the fault.

Table 2. Relationship between the fault classes and the IFBD features.

Types of Short Circuit Faults	Feature Relationship
Three-phase faults	$F_c > F_a > F_b$
Single-phase faults	$F_b > F_a > F_c$
Two-phase faults of *A* and *B*	$F_a > F_b > F_c$
Two-phase faults of *A* and *C*	$F_a > F_c > F_b$
Two-phase faults of *B* and *C*	$F_c > F_b > F_a$

The three phase currents were chosen as the original signals of the online power cable. The IFBD recognition algorithm could be described as follows.

Step 1: Input the three phase currents.
Step 2: Extract the current signals of any phase in fault state, and calculate the traditional box dimensions $Dim(S_A)$, $Dim(S_B)$, and $Dim(S_C)$ of the fault components of phase A, B, and C using Equation (3).
Step 3: Substitute the traditional box dimensions $Dim(S_A)$, $Dim(S_B)$, and $Dim(S_C)$ respectively into Equations (6)–(8) to calculate the improved box dimension features F_A, F_B, and F_C of the fault components of the three phase currents.
Step 4: Classify the short circuit fault according to Table 2.

4. The Developed Maximum Wavelet Coefficient (DMWC) Recognition Algorithm

In this section, we develop the DMWC recognition algorithm for the single-phase grounded faults (DMWCSP) and the two-phase grounded faults (DMWCTP). Similar to the previous IFBD recognition algorithm, the three phase currents were chosen as the original signals of the online power cable for the DMWC recognition algorithm.

In the fault state, the three phase components are asymmetric and interlocked, so the calculation and analyses are complex. After the K-transform below, we obtained the α modulus, the β modulus, and the 0 modulus of the three phases.

$$\begin{cases} i_0 = \frac{1}{3}(i_A + i_B + i_C) \\ i_\alpha = \frac{1}{3}(i_A - i_B) \\ i_\beta = \frac{1}{3}(i_A - i_C) \end{cases} \tag{9}$$

where i_A, i_B, and i_C are the three phase currents of the online power cable.

The modulus components of 0, β, and α for the different faults are shown in Table 3. It can be seen that the different classes of faults correspond to different patterns of the modulus α, modulus β, and the modulus 0. The DMWC algorithm of DMWCSP and DMWCTP are developed below.

Table 3. Modulus components of α, β, and 0 for the different faults.

Type of Fault	Boundary Condition	0 Modulus	α Modulus	β Modulus
Grounded fault of phase A	$i_b = i_c = 0$	i_a	i_a	i_a
Grounded fault of phase B	$i_a = i_c = 0$	i_b	$-i_b$	0
Grounded fault of phase C	$i_a = i_b = 0$	i_c	0	$-i_c$
Phase-between fault of A and B	$i_a + i_b = 0, i_c = 0$	0	$2i_a$	i_a
Phase-between fault of A and C	$i_a + i_c = 0, i_b = 0$	0	$-i_b$	i_b
Phase-between fault of B and C	$i_c + i_b = 0, i_a = 0$	0	i_a	$2i_a$
Grounded faults of A and B	$i_c = 0$	$i_a + i_b$	$i_a - i_b$	i_a
Grounded faults of A and C	$i_b = 0$	$i_a + i_c$	i_a	$i_a - i_c$
Grounded faults of B and C	$i_a = 0$	$i_b + i_c$	$-i_b$	$-i_c$
Grounded fault of A, B, and C	$i_a + i_b + i_c = 0$	0	$i_a - i_b$	$i_a - i_c$

Based on the experiments, the wavelet Db3 were used to analyze the modulus components of α, β, and 0 for the different faults. The maximum wavelet coefficients I_0, I_α, and I_β are listed in Table 4 for the 10 types of short circuit faults. The flow chart of the calculation of the maximum wavelet coefficients [31] is shown in Figure 4.

Table 4. Maximum wavelet coefficients I_0, I_α, and I_β of the different faults.

Fault	I_0	I_α	I_β
Grounded fault of *A*	0.2997	0.2997	0.2997
Grounded fault of *B*	4.5535	4.5535	0.0003
Grounded fault of *C*	4.8586	0.0001	4.8586
Phase-between fault of *A* and *B*	0.0000	4.6010	2.3005
Grounded faults of *A* and *B*	4.5173	4.6010	1.8867
Phase-between fault of *A* and *C*	0.0000	2.7855	5.5721
Grounded faults of *A* and *C*	4.2387	2.0056	5.5721
Phase-between fault of *B* and *C*	0.0001	5.0865	5.0865
Grounded faults of *B* and *C*	0.2786	4.9471	5.2260
Grounded fault of *A*, *B*, and *C*	0.0000	4.6010	5.5721

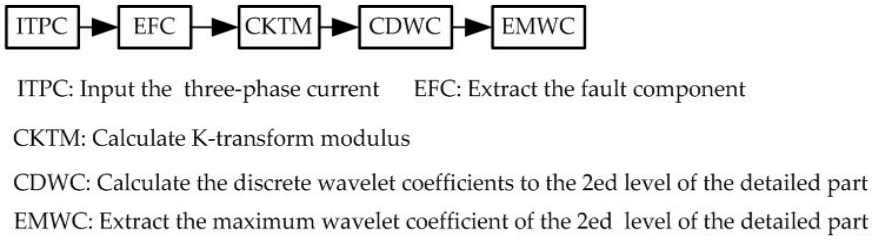

Figure 4. Flow chart of the calculation of the maximum wavelet coefficients.

The proposed DMWCSP algorithm is described below.

Step 1: Calculate the modulus components i_0, i_α, and i_β of the three phase currents i_A, i_B, and i_C by using the K-transform.

Step 2: Calculate the maximum wavelet coefficients I_α and I_β of the modulus components i_α and i_β by using the Wavelet transform.

Step 3: If $I_\alpha < 0.01$, then the fault is classified as the grounded fault of *C*. Otherwise, go to the next step.

Step 4: If $I_\beta < 0.01$, then the fault is classified as the grounded fault of *B*. Otherwise, go to the next step.

Step 5: The fault is classified as the grounded fault of *A*.

Similar to the proposed DMWCSP algorithm, the proposed DMWCTP algorithm was described below to support DMWC recognition algorithm.

Step 1: Calculate the modulus components i_0, i_α, and i_β of the three phase currents i_A, i_B, and i_C by using the K-transform.

Step 2: Calculate the maximum wavelet coefficients I_0 of the modulus components i_0 by using the Wavelet transform.

Step 3: If $I_0 < 0.01$, then the fault is classified as the two-phase grounded fault of *AB*, *AC*, or *BC*. Otherwise, the fault is classified as the two-phase-between fault of *AB*, *AC*, or *BC*.

5. The Proposed Fusion Sensing Method

From the above studies, it was found that the IFBD recognition algorithm could recognize the single-phase fault, double-phase faults, and the three-phase fault easily. Additionally, it had a slight advantage in classifying the detailed single-phase faults of *A*, *B*, and *C*. In contrast, the DMWCSP and DMWCTP algorithms could recognize the detailed single-phase faults of *A*, *B*, and *C*. However, they had relative difficultly in recognizing the detailed double-phase faults of *AB*, *AC*, and *BC*.

The flow chart of the FS method is shown in Figure 5. The FS method is described below.

Step 1: Input the real-time three-phase currents I_A, I_B, and I_C.

Step 2: Extract the fault components i_a, i_b, and ic according to Equation (2).

Step 3: Calculate the improved box dimension features F_A, F_B, and F_C of the fault components of the three phase currents by using Equations (6)–(8).

Step 4: If $F_C > F_A > F_B$, the fault is classified as the three-phase fault. Otherwise, go to the next step.

Step 5: If $F_A > F_B > F_C$, classify the fault as the phase-between fault of AB if $I_0 < 0.01$ or as the two-phase grounded fault of AB if $I_0 > 0.01$. Otherwise, go to the next step.

Step 6: If $F_A > F_C > F_B$, classify the fault as the phase-between fault of AC if $I_0 < 0.01$ or as the two-phase grounded fault of AC if $I_0 > 0.01$. Otherwise, go to the next step.

Step 7: If $F_C > F_B > F_A$, classify the fault as the phase-between fault of BC if $I_0 < 0.01$ or as the two-phase grounded fault of BC if $I_0 > 0.01$. Otherwise, go to the next step.

Step 8: If $F_B > F_A > F_C$, classify the fault as the single-phase grounded fault of C if $I_\alpha < 0.01$ or as the single-phase grounded fault of B if $I_\beta > 0.01$. Otherwise, classify the fault as the single-phase grounded fault of A.

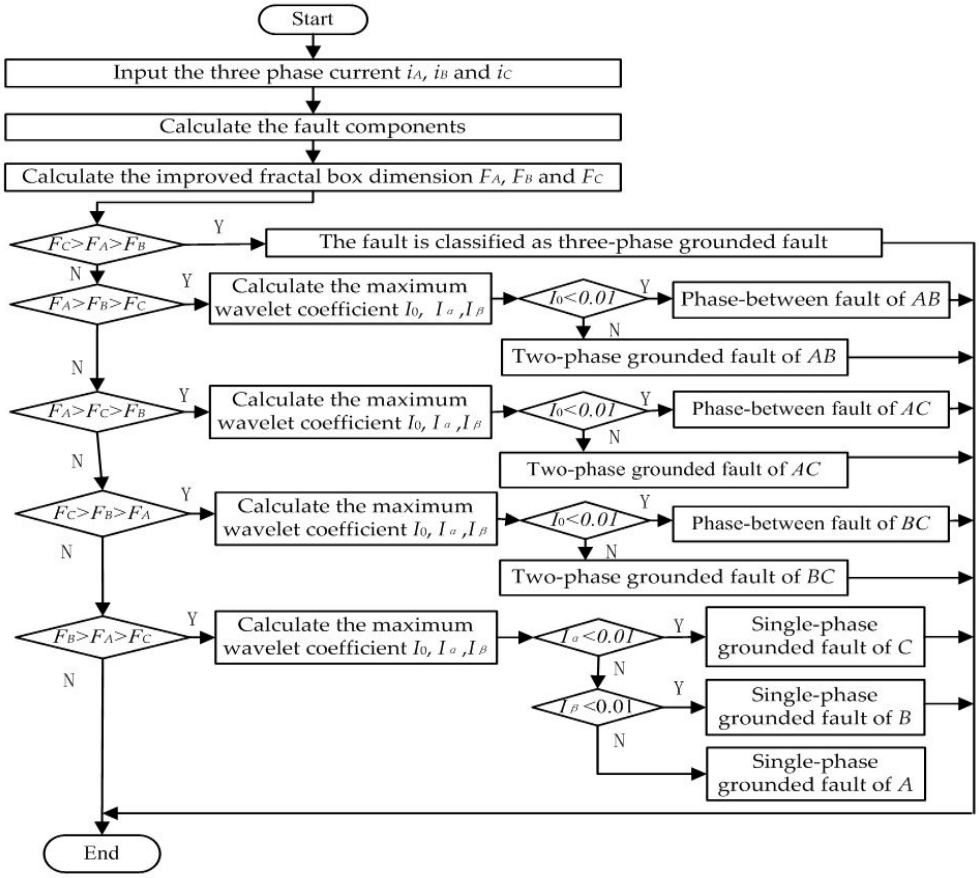

Figure 5. Flow chart of the fusion sensing (FS) method.

6. Experiment and Results

6.1. Experimental Environment

The experimental system structure is shown in Figure 6.

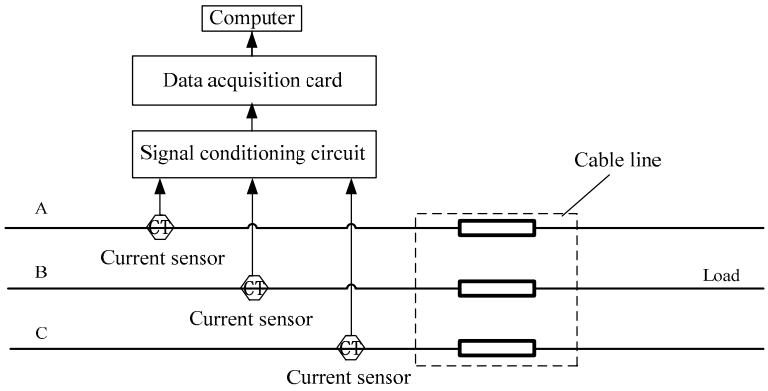

Figure 6. Experimental system structure.

The LabVIEW software was used for the interface platform. The diameter of the power cable was 2.5 mm. The power supply was the three phase variable-frequency power SPS-HL-3300 N, which changed the voltage from 380 V to 90 V.

The star connection mode was used with the neutrals grounded. The signal collection card was a NI PCI-9203. The closed-loop Hoare current sensors CHB-25NP were from Beijing SENSOR Electronics Co., Ltd. (Beijing, China).

6.2. Experiment Results and Analysis

Table 5 shows the IFBD recognition process and the results with an initial angle of 30° and a fault resistance of 30 Ω. Table 6 shows the DMWC recognition process and the results with the initial angle of 30° and fault resistances of 30 Ω and 300 Ω.

Table 5. IFBD recognition with initial angle of 30° and fault resistance of 30 Ω.

$Dim(S_A)$	$Dim(S_B)$	$Dim(S_C)$	F_A	F_B	F_C	Recognition Result
1.56129	1.58036	1.54921	6.20045	6.96163	5.79713	Single-phase grounded fault
1.55953	1.58077	1.54182	6.13833	6.98000	5.57463	Single-phase grounded fault
1.56304	1.58127	1.54840	6.26345	7.00254	5.77191	Single-phase grounded fault
1.47034	1.43155	1.20976	4.04967	3.51537	1.93227	Phase-between fault of *AB*
1.47022	1.43993	1.22141	4.04778	3.61930	1.98314	Two-phase grounded fault of *AB*
1.47985	1.21997	1.44359	4.20460	1.97674	3.66650	Phase-between fault of *AC*
1.47701	1.22034	1.44819	4.15717	1.97838	3.72746	Two-phase grounded fault of *AC*
1.03145	1.43805	1.47034	1.34675	3.59549	4.04967	Phase-between fault of *BC*
1.05752	1.43032	1.46975	1.41522	3.50058	4.04041	Two-phase grounded fault of *BC*
1.16057	1.12408	1.19392	1.73838	1.61290	1.86633	Three-phase grounded fault of *ABC*

Table 6. DMWC recognition with different fault resistances.

Initial Angle	Fault Resistance	I_0	I_α	I_β	Recognition Result
30°	30 Ω	5.3462	5.3462	5.3462	Single-phase grounded fault of *A*
30°	30 Ω	11.8208	11.8208	0.0015	Single-phase grounded fault of *B*
30°	30 Ω	6.4669	0.0105	6.4746	Single-phase grounded fault of *C*
30°	30 Ω	0	20.4730	10.2362	Phase-between fault of *AB*
30°	30 Ω	0	0.6722	1.3458	Phase-between fault of *AC*
30°	30 Ω	0	10.9097	10.9091	Phase-between fault of *BC*
30°	300 Ω	0.8570	0.8571	0.8570	Single-phase grounded fault of *A*
30°	300 Ω	1.8927	1.8927	0.0015	Single-phase grounded fault of *B*
30°	300 Ω	1.0367	0.0105	1.0379	Single-phase grounded fault of *C*
30°	300 Ω	0	2.8251	1.4122	Phase-between fault of *AB*
30°	300 Ω	0	0.0922	0.1857	Phase-between fault of *AC*
30°	300 Ω	0	1.5057	1.5051	Phase-between fault of *BC*

Table 7 shows the comparison of the DMWC recognition method and the FS method with different initial angles 0°, 30°, and 90°, and fault resistances of 30 Ω, 150 Ω, and 300 Ω. Table 8 shows the comparison of the DMWC recognition method and the FS method with different initial angles of 0° and 30°, and different fault distances of 0.8 km, 8 km, and 30 km.

Table 7. Comparison of DMWC and FS with different fault resistances.

Initial Angle	Fault Resistance	Recognition by DMWC	Recognition by FS
0°	30 Ω	91%	97%
0°	150 Ω	86%	96%
30°	30 Ω	88%	95%
30°	150 Ω	79%	93%
90°	30 Ω	75%	98%
90°	150 Ω	72%	98%
90°	300 Ω	71%	97%
Mean value		80.3%	96.3%

Table 8. Comparison of DMWC and FS with different fault distances.

Initial Angle	Fault Distance	Recognition Results by DMWC	Recognition Results by FS
0°	0.8 km	96%	99%
0°	8 km	95%	99%
0°	30 km	92%	98%
90°	0.8 km	85%	98%
90°	8 km	81%	97%
90°	30 km	78%	97%
Mean value		87.8%	98.0%

It can be seen from Table 5 that the IFBD recognition algorithm could classify 8 of the 10 types of short circuit faults. It could recognize the single-phase grounded faults, but could distinguish the detailed fault phase of *A*, *B*, or *C*.

The experiments proved that the DMWC recognition algorithm could correctly classify all 10 types of short circuit faults. In addition, the fault resistances had no influence on the recognition result of the DMWC recognition algorithm. Therefore, this algorithm is better than the IFBD recognition algorithm regarding fault type recognition.

It can be seen from Tables 7 and 8 that the FS method could correctly classify all 10 types of short circuit faults. The initial angle, the fault resistance, and the fault distance had no influence on the recognition result of the FS method. Therefore, the FS method is better than the IFBD recognition algorithm and the DMWC recognition algorithm regarding their comprehensive performances.

7. Conclusions

The IFBD algorithm was developed to enlarge the distances between 10 classes of short circuit faults by using the improved fractal dimension feature extracted from the three-phase currents for the first stage of fault recognition. K-transform and wavelet analysis were then used to establish the relationship between the modulus value and the fault class, and the DMWC recognition algorithm was developed. The IFBD algorithm and the DMWC algorithm were then combined to produce the FS method. Finally, the test system was utilized with the LabVIEW platform. The FS method was experimentally proven to effectively recognize all 10 classes of short circuit faults. The FS method was also not influenced by the parameters of the initial angle, transient resistance, and the fault distance. Compared with the DMWC algorithm, the FS method improved the recognition accuracy from 80.3% to 96.3% in the case of varied fault resistances, and improved the recognition accuracy from 87.8% to 98.0% in the case of varied fault distances.

Acknowledgments: This research was sponsored by the Natural Science Foundation of China (51405381), the Key Scientific and Technological Project of Shaanxi Province (2016GY-040), and the Science Foundation of Xi'an University of Science and Technology (104-6319900001).

Author Contributions: M.W. conceived and designed the experiments; L.Z. and Y.G. performed the experiments; M.W. and L.Z. and Y.G. analyzed the data; M.W. and L.Z. and Y.G. wrote the paper.

Conflicts of Interest: The authors declare no conflict of interest.

References

1. Zhao, J.H.; Xu, Y.; Luo, F.J.; Dong, Z.Y.; Peng, Y.Y. Power system fault diagnosis based on history driven differential evolution and stochastic time domain simulation. *Inf. Sci.* **2014**, *275*, 13–14. [CrossRef]
2. Prasad, A.; Edward, J.B. Application of Wavelet Technique for Fault Classification in Transmission. *Procedia Comput. Sci.* **2016**, *92*, 78–81. [CrossRef]
3. Jun, J.T.; Feng, P.F.; Wei, S.L.; Zhang, H.; Liu, Y.F. Investigation on the surface morphology of Si_3N_4 ceramics by a new fractal dimension calculation method. *Appl. Surf. Sci.* **2016**, *387*, 813–817.
4. Guclu, S.O.; Ozcelebi, T.; Lukkien, J. Distributed Fault Detection in Smart Spaces Based on Trust Management. *Procedia Comput. Sci.* **2016**, *83*, 66–70. [CrossRef]
5. Bharata, M.J.; Gopakumar, P.; Mohanta, D.K. A novel transmission line protection using DOST and SVM. *Eng. Sci. Technol.* **2016**, *19*, 1027–1037.
6. Lin, S.; Mei, J.T.; Chen, S.; He, Z.Y.; Qian, Q.Q. Fault Detection and Faulty Phase Determination of Transmission Lines Based on Time-Frequency Characteristics of Transient Travelling Waves. *Power Syst. Technol.* **2012**, *36*, 49–52.
7. Chicharro, F.I.; Cordero, A.; Torregrosa, J.R. Dynamics and Fractal Dimension of Steffensen-Type Methods. *Algorithms* **2015**, *8*, 271–279. [CrossRef]
8. Gómez, M.J.; Castejón, C.; García-Prada, J.C. Review of Recent Advances in the Application of the Wavelet Transform to Diagnose Cracked Rotors. *Algorithms* **2016**, *9*, 19. [CrossRef]
9. Zhou, W.; Xiong, J.; Li, F.; Jiang, N.; Zhao, N. Fusion of Multiple Pyroelectric Characteristics for Human Body Identification. *Algorithms* **2014**, *7*, 685–702. [CrossRef]
10. Tan, X.H.; Liu, J.Y.; Li, X.P.; Zhang, L.H.; Cai, J.C. A simulation method for permeability of porous media based on multiple fractal model. *Int. J. Eng. Sci.* **2015**, *95*, 76–80. [CrossRef]
11. Yu, M.Z.; Chan, T.L. A bimodal moment method model for submicron fractal-like agglomerates undergoing Brownian coagulation. *J. Aerosol Sci.* **2015**, *88*, 25–30. [CrossRef]
12. Martino, G.D.; Iodice, A.; Riccio, D.; Ruello, G.; Zinno, I. Angle Independence Properties of Fractal Dimension Maps Estimated From SAR Data. *IEEE J. Sel. Top. Appl. Earth Obs. Remote Sens.* **2013**, *6*, 1242–1248. [CrossRef]
13. Nelson, J.D.B.; Kingsbury, N.G. Fractal dimension, wavelet shrinkage and anomaly detection for mine hunting. *IET Signal Process.* **2012**, *6*, 485–487. [CrossRef]
14. Reza, F.M.; Qi, X.J. Face Recognition under Varying Illumination with Logarithmic Fractal Analysis. *IEEE Signal Process. Lett.* **2014**, *21*, 1459–1460.
15. Xu, Y.; Liu, D.L.; Quan, Y.H.; Callet, P.L. Fractal Analysis for Reduced Reference Image Quality Assessment. *IEEE Trans. Image Process.* **2015**, *24*, 2099–2100. [CrossRef] [PubMed]
16. Tumu, I.; Concas, G.; Marchesi, M.; Tonelli, R. The fractal dimension of software networks as a global quality metric. *Inf. Sci.* **2013**, *245*, 295–299.
17. Liu, J.H.; Liang, R.; Wang, C.L.; Fan, D.P. Application of fractal theory in detecting low current faults of power distribution system in coal mines. *Min Sci. Technol. (China)* **2009**, *19*, 321–323. [CrossRef]
18. Usama, Y.; Liu, X.M.; Imam, H.; Sen, C.; Kar, N.C. Design and implementation of a wavelet analysis-based shunt fault detection and identification module for transmission lines application. *IET Gener. Transm. Distrib.* **2014**, *8*, 431–440. [CrossRef]
19. Zhang, S.W.; Zhang, F.; Wang, Z.J.; Gu, H.Y.; Ning, Q. Series Arc Fault Identification Method Based on Energy Produced by Wavelet Transformation and Neural Network. *Trans. China Electrotech. Soc.* **2014**, *29*, 291–293.
20. Gopakumar, P.; Reddy, M.J.B.; Mohanta, D.K. Transmission line fault detection and localisation methodology using PMU measurements. *IET Gener. Transm. Distrib.* **2015**, *9*, 1033–1039. [CrossRef]

21. Zhang, L.L.; Xu, B.Y.; Xue, Y.D.; Gao, H.L. Transient Fault Locating Method Based on Line Voltage and Zero-mode Current in Non-solidly Earthed Network. *Proc. CSEE* **2012**, *32*, 110–113.
22. Prasad, A.; Edward, J.B. Application of Wavelet Technique for Fault Classification in Transmission Systems. *Procedia Comput. Sci.* **2016**, *92*, 78–83. [CrossRef]
23. Dai, H.Z.; Zheng, Z.B.; Wang, W. A new fractional wavelet transform. *Commun. Nonlinear Sci. Numer. Simul.* **2017**, *44*, 19–32. [CrossRef]
24. Wu, Q.; Law, R. Complex system fault diagnosis based on a fuzzy robust wavelet support vector classifier and an adaptive Gaussian particle swarm optimization. *Inf. Sci.* **2010**, *180*, 4515–4520. [CrossRef]
25. Zheng, G.P.; Zhang, L.; Jiang, C.; Qi, Z.; Yang, Y.H. Line and Segment Online Location of Single-phase-to-earth Fault in the Ungrounded Neutral System. *Autom. Electr. Power Syst.* **2013**, *37*, 111–113.
26. Jiang, J.A.; Chuang, C.L.; Wang, Y.C.; Hung, C.H.; Wang, J.Y.; Lee, C.H.; Hsiao, Y.T. A Hybrid Framework for Fault Detection, Classification, and Location—Part I: Concept, Structure, and Methodology. *IEEE Trans. Power Deliv.* **2011**, *26*, 1990–1998. [CrossRef]
27. Tang, G.; Hou, W.; Wang, H.Q.; Luo, G.G.; Ma, J.W. Compressive Sensing of Roller Bearing Faults via Harmonic Detection from Under-Sampled Vibration Signals. *Sensors* **2015**, *15*, 25648–25660. [CrossRef] [PubMed]
28. Wook, K.J.; Kim, J.H.; Seo, J. Multiple Leader Candidate and Competitive Position Allocation for Robust Formation against Member Robot Faults. *Sensors* **2015**, *15*, 10777–10780.
29. Han, C.; Zhang, H.Y.; Guo, C.X.; Jiang, C.; Sang, N.; Zhang, L.P. A Remote Sensing Fusion Method Based on the Analysis Sparse Model. *IEEE J. Sel. Top. Appl. Earth Obs. Remote Sens.* **2016**, *9*, 1302–1308. [CrossRef]
30. Xu, J.D.; Yu, X.C.; Pei, W.J.; Hu, D.; Zhang, L.B. A remote sensing fusion method based on feedback sparse component analysis. *Comput. Geosci.* **2015**, *85*, 116–118. [CrossRef]
31. Cheng, J.; Liu, H.J.; Liu, T.; Wang, F.; Li, H.S. Remote sensing image fusion via wavelet transform and sparse representation. *ISPRS J. Photogramm. Remote Sens.* **2015**, *104*, 160–170. [CrossRef]